\$ SUPER

Contents lists available at ScienceDirect

International Journal of Applied Earth Observation and Geoinformation

journal homepage: www.elsevier.com/locate/jag





The novel triangular spectral indices for characterizing winter wheat drought

Fu Xuan ^{a,b}, Hui Liu ^{a,b}, JingHao Xue ^c, Ying Li ^{d,e}, Junming Liu ^{a,b}, Xianda Huang ^{a,b}, Zihao Tan ^{a,b}, Mohamed A.M. Abd Elbasit ^f, Xiaohe Gu ^g, Wei Su ^{a,b,*}

- ^a College of Land Science and Technology, China Agricultural University, Beijing 100083, China
- ^b Key Laboratory of Remote Sensing for Agri-Hazards, Ministry of Agriculture and Rural Affairs, Beijing 100083, China
- ^c Department of Statistical Science, University College London, London WC1E 6BT, UK
- ^d CMA Henan Agrometeorological Support and Applied Technique Key Laboratory, Zhengzhou 450003, China
- e Henan Institute of Meteorological Sciences, Zhengzhou 450003, China
- f School of Natural and Applied Sciences, Sol Plaatje University, Kimberley 8301, South Africa
- g Research Center of Information Technology, Beijing Academy of Agriculture and Forestry Sciences, Beijing 100097, China

ARTICLE INFO

Keywords: Triangular spectral indices Agricultural drought Three-dimensional feature space ECHI. PWSI. DCHI

ABSTRACT

Agricultural drought threatens food security and agricultural sustainable development. There have been numerous spectral indices from remote sensing images developed for monitoring crop drought. However, most present spectral indices are focusing on crop growth and Land Surface Temperature (LST), and the crop canopy water content are in less consideration simultaneously. Additionally, the Normalized Difference Vegetation Index (NDVI) is used for characterizing crop growth in almost all spectral drought indices, with the spectral saturation problem of NDVI for closed crop canopy. When vegetation cover is high, NDVI values tend to saturate, which makes them insensitive to further changes in crop health. Therefore, the NDVI saturation phenomenon may lead to an underestimation of the extent of crop drought, as it is not effective in identifying subtle changes in crops under high-density vegetation conditions. Hence, we propose three novel triangular spectral indices for characterizing winter wheat drought using three features including LAI, Land Surface Water Index (LSWI) and LST. For validating the proposed spectral indices, we compared the agreement between these indices with measured Relative Soil Moisture (RSM) and Volumetric Water Content (VWC) of soil in agricultural meteorological station and present popular indices including Crop Water Stress Index (CWSI), Temperature-Vegetation Drought Index (TVDI), and Vegetation Health Index (VHI). The results revealed that our proposed indices including Euclidean distance Crop Health Index (ECHI), Difference Crop Health Index (DCHI) and Perpendicular Water Stress Index (PWSI) outperformed the popular CWSI, TVDI and VHI, with stronger correlations with measured RSM and VWC in agricultural meteorological station. Secondly, there are spatial consistencies for characterizing winter wheat drought between proposed ECHI, DCHI and PWSI with popular CWSI, TVDI and VHI. In addition, our proposed ECHI, DCHI and PWSI have achieved good performance of drought monitoring both in irrigated and rainfed croplands. All these results suggest that our proposed indices have great potential in crop drought monitoring.

1. Introduction

Drought is a pervasive and complex hazard for crop failures (Yihdego et al., 2019; Azmi et al., 2016; Sheffield and Wood, 2012), which will lead to yield and economic loss and threaten agricultural sustainable development (Lesk et al., 2022). Wheat is one of the three main grains (rice, corn and wheat) in China. Henan province is the largest producer of winter wheat in China, with the planted area of 5706.65 thousand

hectares and the yield of 37.48 million tons in 2019. Drought has brought serious impacts on agricultural production. In the spring of 2019, the area affected by drought was 64.2 thousand hectares, the area of lost harvest was 6.8 thousand hectares, resulting in agricultural losses of 286 million yuan in Henan Province (Henan Provincial Bureau of Statistics, 2019). Globally, agricultural drought poses significant threats to food security, economic stability, and sustainable development. According to the Food and Agriculture Organization (FAO), droughts have

E-mail address: suwei@cau.edu.cn (W. Su).

^{*} Corresponding author.

affected more than 1.5 billion people from 2000 to 2019, causing substantial economic losses and exacerbating food insecurity (FAO, 2023). These global impacts highlight the importance of improving drought monitoring techniques to mitigate its adverse effects on agriculture. Therefore, the efficient and accurate monitoring of agricultural drought is vital for agricultural sustainable development.

There are four kinds of drought including meteorological drought, agricultural drought, hydrological drought and socio-economic drought (Wilhite and Glantz, 1985). Agricultural drought is the period of soil water deficit caused by lower precipitation and higher evaporation and transpiration (Dai, 2011), which is the most severe meteorological disaster affecting agricultural production. Remote sensing is extensively used for agricultural drought monitoring for its good performance on acquiring the data of crop and cropland quickly in large area with low cost (Huang et al., 2019; Mehmood et al., 2024b; Xuan et al., 2023). This technology enables the continuous observation of crop conditions and soil moisture levels, providing critical information that can be used to assess the severity, temporal change, and spatial distribution of drought. The spectral drought indices derived from remote sensing data are particularly useful for quantifying drought characteristics, allowing for more precise and dynamic monitoring of agricultural drought. Furthermore, remote sensing facilitates the integration of multiple data sources, including satellite imagery, ground-based observations, and climate models, to provide a comprehensive understanding of drought conditions. This integration is essential for developing effective drought mitigation strategies and ensuring sustainable agricultural practices. In summary, the ability of remote sensing to provide timely, highresolution, and broad-scale data makes it especially suited for agricultural drought monitoring (Anees et al., 2024; Mehmood et al., 2024a). Developing the efficient spectral drought indices do good to drought monitoring by describing the severity, temporal change and spatial distribution of drought by quantifying drought characteristics.

The existing spectral drought indices can be classified into four groups (Hao and Singh, 2015) including (1) soil drought indices, such as Soil Moisture Index (SMI) (Esch et al., 2018) and Ratio Dryness Monitoring Index (RDMI) (Zhang et al., 2019); (2) vegetation drought indices, such as Vegetation Condition Index (VCI) and Enhanced Vegetation Index (EVI) (Ha et al., 2023; Shi et al., 2022; Dubovyk et al., 2019); (3) temperature drought indices, such as Land Surface Temperature (LST) (Gutman, 1990) and Thermal Condition Index (TCI) obtained from longterm LST (Kogan, 1995). Soil-vegetation drought indices such as Visible and Short-wave infrared Drought Index (VSDI) (Zhang et al., 2013), Normalized Multi-band Drought Index (NMDI) (Wang et al., 2008), and Short-wave Infrared Water Stress Index (SIWSI) (Fensholt and Sandholt, 2003) have been proposed to address the monitoring challenges in semiarid regions with sparse vegetation. Vegetation-temperature drought indices including Temperature-Vegetation Drought Index (TVDI) (Sandholt et al., 2002), Vegetation Temperature Condition Index (VTCI) (Sandholt et al., 2002), and Vegetation Health Index (VHI) (Abbass et al., 2022), combine remote sensing of land surface temperature with the growth status of vegetation as drought indicators. Meanwhile, vegetation-temperature-water content drought indices like Temperature Vegetation Shortwave Infrared Reflectance Dryness Index (TVSDI) (Xu et al., 2022), Temperature Vegetation Water Stress Index (TVWSI) (Joshi et al., 2021), and Temperature Vegetation Precipitation Dryness Index (TVPDI) (Wei et al., 2020) assess the drought responses by combining two elements from evapotranspiration, vegetation growth and soil moisture (Joshi et al., 2021). Unfortunately, there is still challenges of these indices for agricultural drought monitoring. Firstly, the crop canopy structure changes significantly from open canopy to closed canopy, and the NDVI will be saturated after the canopy is closed. This problem will result in the low performance of drought monitoring using NDVI (Dong et al., 2021; Ma Rufah et al., 2017; Zhang et al., 2017). Moreover, the 2D drought indices take into account less crop canopy water content at the same time. Current indices are unable to monitor the full range of characteristics of crop water deprivation or address

spectral saturation, limitations that highlight the need for the development of a new spectral drought index. Improved indices should be able to capture more detailed information on crop canopy structure, moisture content and overall vegetation health to provide more reliable and accurate drought monitoring.

To overcome the limitations of existing remote sensing drought indices, we try to develop triangular spectral indices using LAI, LSWI and LST (or SWIR reflectance) for monitoring winter wheat drought. The LAI is the proxy of crop growth, instead of NDVI for alleviating the saturation problem after the crop canopy is closed. Combination of LSWI is done for quantifying the crop canopy water content. And LST or SWIR is used for characterizing crop canopy temperature. These three parameters are used to build 3D feature space, ECHI, DCHI and PWSI are built within this 3D feature space. The objective of this study is to develop the triangular spectral indices and validate their performance with measured soil water content in agricultural meteorological station and existing popular indices. Furtherly, our proposed spectral drought indices are explored to characterize the winter wheat drought in a complete drought period and compared the performance of drought monitoring in both irrigation and rainfed cropland.

2. Study area and data sources

2.1. Study area

The study area is in Henan Province, located in the central-east of China. The topography of Henan Province is predominantly characterized by plains and basins, and the landforms of Henan Province can be divided into five regions, namely, the Huanghuaihai Plain, which accounts for nearly 50 % of the total area of the province; the northern mountains, where there are one-sided mountains with an elevation of about 1,500 m, and hills with an elevation of 300-400 m in front of the mountains; the western mountains, where the elevation of the mountains is generally 500-2,000 m; the Nanyang Basin, which is situated at an elevation of 80–150 m between the western and southern mountains; and the southern mountains, which are mostly about 800 m in elevation. The Yellow River runs through the entire province from west to east, providing abundant irrigating water sources. Henan Province falls within the warm temperate continental monsoon climate zone. This region experiences hot and rainy summers, cold and dry winters, and short spring and autumn. The annual average temperature ranges between 12-16 °C, and the annual precipitation is varied between 500-1000 mm. Influenced by the monsoon, the rainfall is mainly in summer and autumn when it is the growing season of corn. The frost-free period extends from 201 to 285 days throughout the whole year. And the main crops planted in Henan Province include wheat, corn, cotton, peanuts, rapeseed, rice, and soybeans. Specially, the wheat production of Henan Province ranks first where is vital for food security of China.

Unfortunately, the crop production in Henan Province also faces severe natural challenges including drought, dry hot wind and flood. Spring droughts particularly occurred, as the insufficient rainfall coupled with the increasing temperature, coupling of which accelerates soil moisture evaporation, leading to water stress for winter wheat. Therefore, we are aiming at finding the efficient way to monitor the drought of winter wheat in this study. And the planted area of winter wheat come from the classification products of Huang et al. (2022) and Zhang et al., (2022).

2.2. Data sources

2.2.1. MODIS products

The MODIS (Moderate Resolution Multispectral Imager) is carried aboard both the Terra and Aqua satellites as a part of the U. S. Earth Observing System (EOS). The MODIS hosts the surface reflectance, surface temperature, LAI, and evapotranspiration products, which have been leveraged through the Google Earth Engine (GEE) platform. The

LSWI and SWIR (SWIR2 band) data were derived from the daily gridded L2G product of MOD09GA.061 using the sinusoidal projection, which were used for building our proposed triangular spectral indices. This dataset encompasses 500 m reflectance values and 1 km observation and geolocation statistics. Meanwhile, the LST data was sourced from MOD11A1.061, furnishing daily LST and emissivity values at a spatial resolution of 1000 m. This dataset includes both daytime and night time LST values accompanied by a quality layer. For the spatial consistency, the daytime LST data was resampled to the spatial resolution of 500 m. The LAI data was extracted from MCD15A3H.061. In this process, the "best" pixel available was selected from all the acquisitions within every 4-day period, and the data was captured at a resolution of 500 m. The NDVI data from MOD09GA.061 was used to calculate the TVDI and VHI. And the ET and PET data were acquired from the MOD16A2.061 dataset hosted on the Terra satellite, which were produced using Penman-Monteith equation. These three kinds of MODIS products were used to calculate the TVDI, VHI, and CWSI, for validating our proposed triangular spectral indices to monitor crop drought.

2.2.2. Meteorological data and irrigation products

Measured VWC and RSM at the topsoil depth of 20 cm were collected from 190 meteorological stations in Henan Province for every day of March 2019. These measurements collected on at 6:00 am (UTC) were used to validate our proposed spectral drought indices. The datasets were produces with the spatial resolution of 500 m. The irrigation data were derived from annual distribution mapping of irrigated cropland in China with 500 m spatial resolution, produced by Zhang et al. (2022a; 2022b). These products have demonstrated an overall accuracy ranging from 70 % to 90 % in ground sample validation across the country. In this study, the maps of irrigated and rainfed areas in Henan Province were used to explore the performance of our proposed spectral indices used for drought monitoring in both irrigation and rainfed cropland. (Fig. 1).

3. Methodology

3.1. Conceptual prototype of proposed triangular spectral indices

Drought stress would affect crop leaf photosynthesis, stomatal movement, and nutrient metabolism negatively, limiting the crop

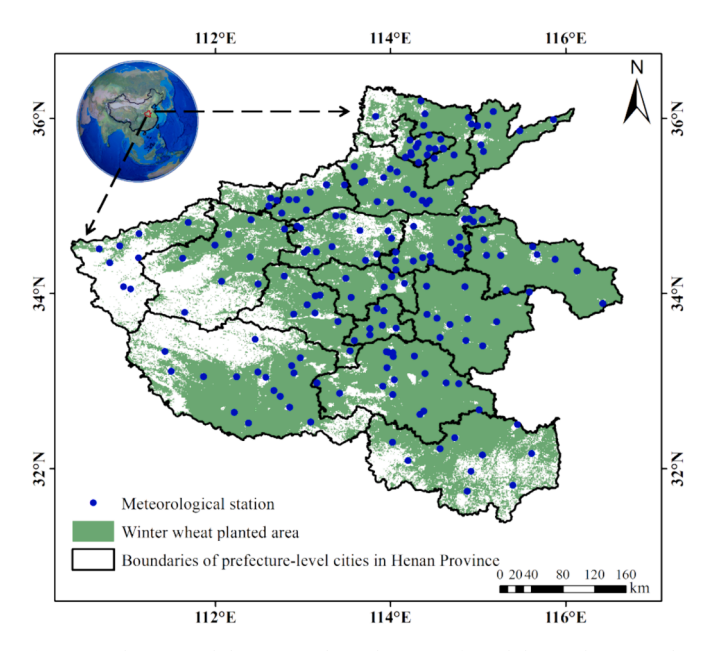


Fig. 1. Study area and the meteorological stations for validating the triangular spectral indices proposed in this study.

growing furtherly. The resulted structural and biological changes from drought included leaf curled, leaf temperature increasing, stomatal conductance and water content decreasing (Li et al., 2013). Inadequate moisture availability inhibits crop growth, and this limitation is directly reflected in vegetation cover, which can lead to a reduction in LAI. LAI is a crucial parameter that represents the total leaf area relative to the ground surface area. A decrease in LAI indicates a reduction in the overall leaf surface available for photosynthesis and transpiration. This reduction in leaf area decreases the canopy's ability to intercept solar radiation, leading to a further decline in canopy water content. The canopy water content can be effectively estimated using the LSWI, which is directly related to the canopy water content. The reduction in canopy water content due to drought stress affects photosynthesis and transpiration processes, leading to an increase in canopy temperature. This temperature rise can be monitored using LST measurements. Under drought conditions, crops mitigate water loss through transpiration by regulating stomatal conductance-closing or narrowing stomata. This physiological response reduces water vapor exchange between the canopy and the atmosphere, resulting in decreased vegetation water content and increased values in the SWIR band. The SWIR band is sensitive to changes in leaf water content, and increases in SWIR reflectance are indicative of reduced water content. As such, LSWI serves as an indicator of the canopy's water status. Fig. 2 illustrates these processes and how they interrelate. Therefore, in this study, we use LAI, LSWI, LST, and SWIR to develop our triangular spectral indices. These indices are designed to capture the complex interactions between canopy structure, water content, and temperature, providing a comprehensive approach to monitoring agricultural drought.

3.2. Derivation of ECHI, PWSI, DCHI in 3D features space

3.2.1. Normalization of images features

Regarding to the biophysical changing process of crop canopy when water deficit happened, the reduction in LAI, the decrease in LSWI, and the increase in LST or SWIR can collectively indicate the impact of water deficiency on vegetation. LAI, LSWI and LST or SWIR were used to develop the triangular spectral indices and characterize the agricultural drought from crop growth. Given there were different value ranges for LAI (0.1-6.8), LSWI (-1.31-0.55) and LST (3.4-31.6 °C) or SWIR (0.0048-0.7016), we normalized all of them to a uniform rang [0,1] symbolized as LAI', LSWI' and LST' or SWIR'. This normalization was essential to ensure comparability among the indices, as it places all parameters on a common scale, facilitating the integration and interpretation of the data. The choice of the [0,1] range for normalization is particularly advantageous because it standardizes each variable into a consistent scale, which simplifies the mathematical manipulation and comparison of different datasets. By converting all measurements to this normalized range, we eliminate the influence of differing units and scales among the original data. This approach is widely used in remote sensing and environmental modeling to ensure that each parameter contributes equally to the final analysis irrespective of its original magnitude (Fang et al., 2019; Li et al., 2024; Luo et al., 2024). These normalized indices were then used to build a feature cube with a length, width, and height of 1. Any points within the 3D coordinates of LAI', LSWI', and LST' or SWIR' would fall into this feature cube (Fig. 3). This feature cube allows for a comprehensive spatial representation of the combined effects of LAI, LSWI, and LST or SWIR on drought characterization.

$$X_{norm}^{i} = \frac{X^{i} - X_{min}^{i}}{X_{max}^{i} - X_{min}^{i}}$$
 (1)

where i is 1–4, representing LAI, LSWI, LST, and SWIR respectively, and X_{norm}^i represents the normalized value, X_{max}^i represents the max value, X_{min}^i represents the min value.

Time-series MODIS images in growing season of winter wheat

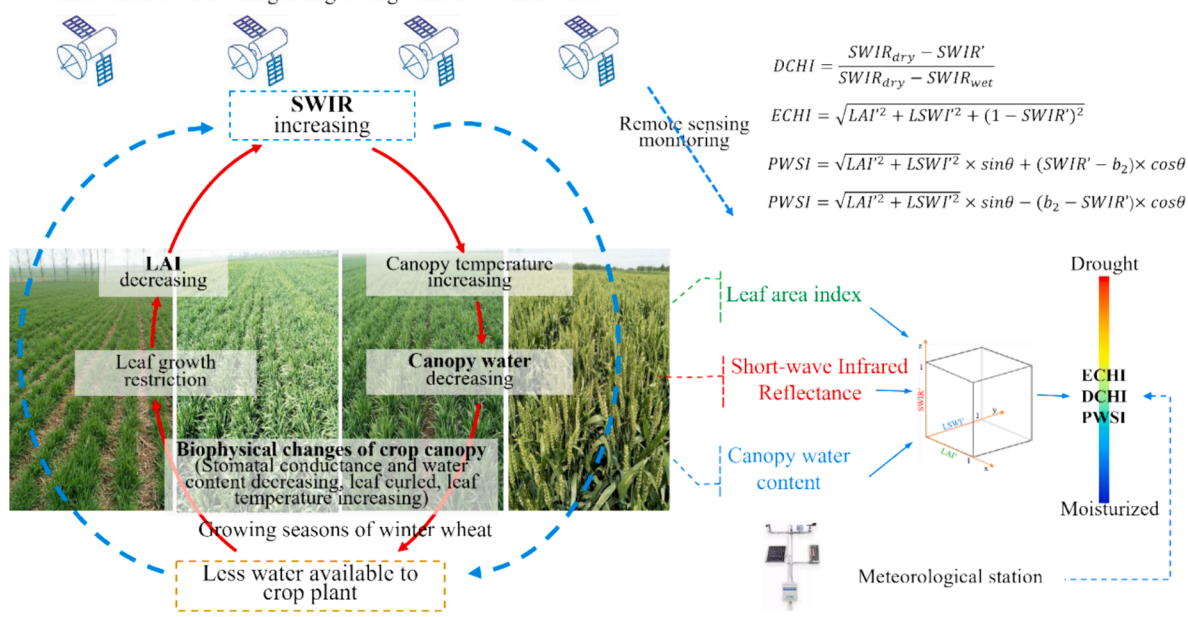


Fig. 2. Conceptual illustration for the proposed triangular spectral indices for drought monitoring.

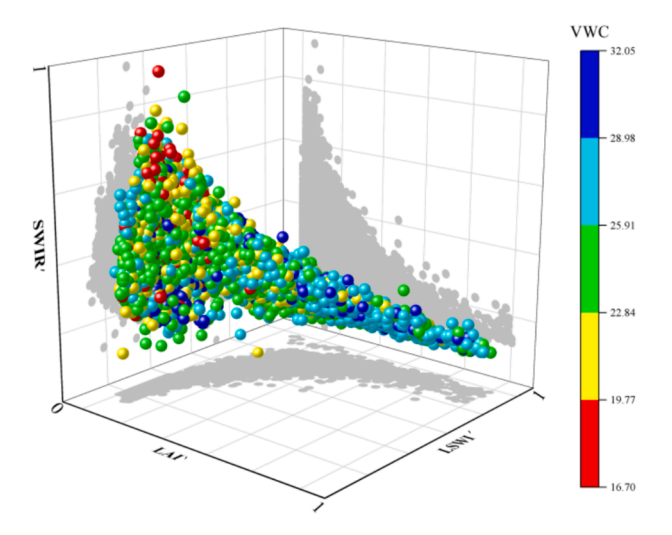


Fig. 3. The 3D feature space of LAI', LSWI' and SWIR' (Gray color represents the projection of the point in each dimension).

3.2.2. Derivation of ECHI

According to the relationship between LAI', LSWI', LST' or SWIR' and drought, it can be deduced that the pixel with smaller LAI', lower LSWI' and higher LST' or SWIR' is probably in drought stress of crop. Conversely, a pixel with higher LAI', lower SWIR' or LST', and higher LSWI' indicates a wetter condition. Within the feature cube shown in Fig. 4, M is a proxy of dry low-vegetation cover area, and point N is a proxy of the full vegetation coverage with saturated water content. The near neighbor of M (0,0,1) would be decided as drought, and the near neighbor of N (1,1,0) would be decided as the most moisturized cropland. Therefore, the distance of given point to the driest D point in this 3D feature space is used to develop ECHI for characterizing the agricultural drought, which is as formula (2). ECHI₁ is calculated within SWIR'-LAI'-LSWI' feature space, ECHI₂ is calculated within LST'- LAI'-LSWI' feature space, and the value of them range from 0 to $\sqrt{3}$.

$$ECHI = \sqrt{LAI^{2} + LSWI^{2} + (1 - SWIR'orLST')^{2}}$$
 (2)

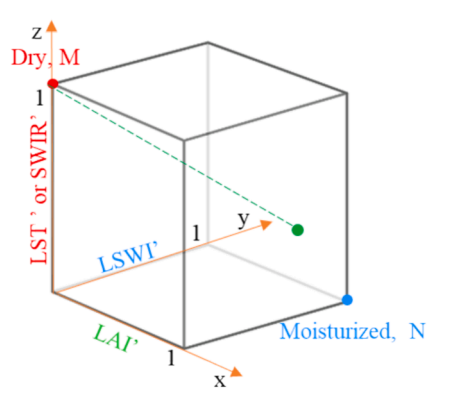


Fig. 4. Derivation illustration of ECHI.

3.2.3. Derivation of DCHI

It could be observed that the trend of LAI is correlated positively with LSWI, LAI and LSWI are all correlated negatively with LST or SWIR from the two-dimensional feature spaces formed by each pair of the three parameters (as depicted by the projections of pixels of the triangular spectral indices onto the three respective planes in Fig. 4). Numerous studies have suggested that a combination of surface temperature, NDVI and canopy temperature (Ts) can provide information on vegetation stress and moisture conditions at the surface. The scatter plots of remotely sensed surface temperature and the NDVI often exhibit triangular or trapezoidal (Carlson et al., 1994; Moran et al., 1994) shapes and are called the NDVI-T_s space. By extracting the plane where the diagonal MN is located, the projection of each point on this plane can also be abstracted as a trapezoid. So, the change of drought severity could be quantified using the simplified two-dimensional feature space of LST or SWIR with $\sqrt{LAI'^2 + LSWI'^2}$, which is shown as the plane in Fig. 5 (a) with the hotspot close to the dry M. And Fig. 5 (b) is the proxy of the plane for characterizing drought severity. Meanwhile, like TVDI (temperature/vegetation dryness index) (Carlson et al., 1994), we can fit the dry and wet edges, assuming that all points are inside the trapezoidal interior. In Fig. 5, point A has the highest LST or SWIR and the lowest LAI and LSWI, so it is assumed to be a dry low-vegetation cover area,

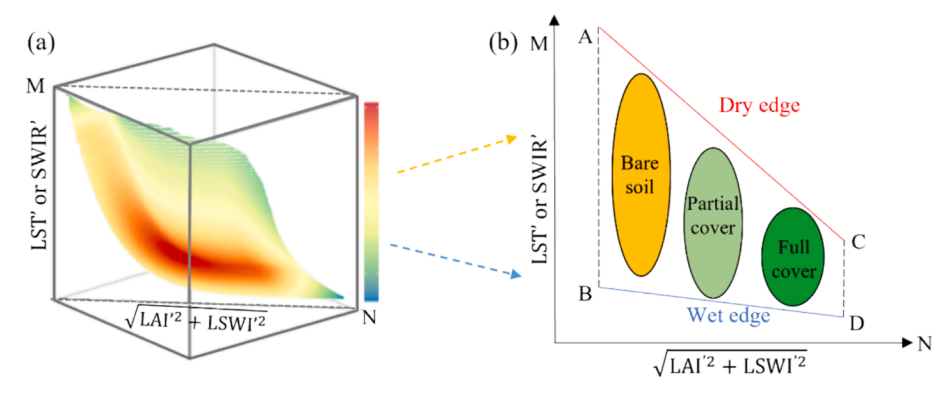


Fig. 5. Deriving DCHI from predigested feature space.

point B has the lowest LST or SWIR and the lowest LAI and LSWI, so it is assumed to be a low-vegetation cover area with saturated moisture content, and similarly point C is assumed to be the water stress under full vegetation cover (vegetation wilting point), and point D represents the area of full vegetation cover at saturated moisture content. The line AC is assumed to be the extreme dry edge (SWIR_{dry}) with poor soil moisture availability and low evapotranspiration, while the line BD means sufficient soil moisture and high surface evapotranspiration, assumed as the extreme wet edge (SWIR_{wet}). According to Sturges (1926), the number of boxes E is calculated using range R and quantity Q, and the highest and lowest LST or SWIR are determined in each box of $\sqrt{\text{LAI}'^2 + \text{LSWI}'^2}$. By fitting the linear regression function, the dry edge and wet edge would be acquired. Where, a_1 and b_1 , a_2 and b_2 are the fitted coefficients of dry edge and wet edge respectively.

$$E = \frac{R}{1 + 3.322\log Q} \tag{3}$$

$$SWIR_{dry} = b_1 + a_1 \times \sqrt{LAI'^2 + LSWI'^2}$$
(4)

$$SWIR_{wer} = b_2 + a_2 \times \sqrt{LAI^2 + LSWI^2}$$
 (5)

Based on the position of pixel within the SWIR $'-\sqrt{LAI'^2+LSWI'^2}$ feature space, DCHI (formula 6) was built to quantify crop drought stress. It represents the ratio between the difference 'm' of SWIR_{dry} and SWIR and the difference 'n' of SWIR_{dry} and SWIR_{wet}. The smaller ratio indicates the closer to the dry edge, the closer the pixel is to the dry edge, indicating a more severe drought condition (Fig. 6). Mathematically, DCHI encapsulates the gradient of dryness, being 0 at the dry edge

where drought conditions are most extreme, and reaching 1 at the wet edge, indicative of no drought stress. Hence, lower DCHI values denote higher levels of drought severity, providing a quantitative measure that aligns with intuitive understandings of drought intensity.

$$DCHI = \frac{m}{n} = \frac{SWIR_{dry} - SWIR'}{SWIR_{dry} - SWIR_{wet}}$$
(6)

3.2.4. Derivation of PWSI

In the 3D feature space illustrated in Fig. 4, pixels close to the dry edge epitomized the severest drought conditions, while those on the wet edge embodied the peak of moisture abundance. Capitalizing on this spatial layout, PWSI and DCHI are built by measuring the perpendicular distance from the given pixel to the wet edge, which was used to quantify the drought stress in crops and its intensity. As shown in Fig. 7, the magnitude of PWSI is contingent on the length of segment OP, which symbolizes the discrepancy between the crop condition represented by the pixel and the extreme moist state. A larger OP corresponds to a higher PWSI value, indicating that the pixel is farther from the wet edge and thus signifies a more severe level of crop drought. Conversely, a smaller OP equates to a lower PWSI value, signifying closeness to the wet edge and thereby inferring milder drought conditions for the crops depicted. Contrary to DCHI, PWSI value is 0 on the wet edge and 1 on the dry edge. The calculation of PWSI varies depending on the relative magnitude of SWIR' or LST' compared to the intercept b2 of the fitted equation delineating the wet edge, which is as formula 7.

$$\theta = \arctan(|\mathbf{a}_2|) \tag{7}$$

$$PWSI = \begin{cases} AB + CP = \sqrt{LAI^2 + LSWI^2} \times \sin\theta + (LST'orSWIR' - b_2) \times \cos\theta, LST'orSWIR' > b_2 \\ EF - EG = \sqrt{LAI'^2 + LSWI'^2} \times \sin\theta - (b_2 - LST'orSWIR') \times \cos\theta, LST'orSWIR' < b_2 \end{cases}$$

$$(8)$$

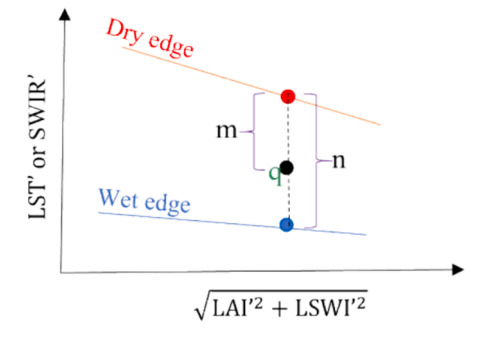


Fig. 6. Derivation illustration of DCHI.

3.3. Evaluation of ECHI, DCHI and PWSI for drought monitoring

Our proposed ECHI, DCHI and PWSI are validated by comparing with measured soil water content in agricultural meteorological stations and existing popular drought indices including CWSI, TVDI and VHI. The CWSI is used to validate the capabilities of meteorological drought monitoring, while the TVDI and VHI are used to validate the capabilities of remote sensing drought monitoring. The correlation between ECHI, DCHI and PWSI with the measured soil VWC are analyzed to for validation of drought monitoring. Pearson Correlation Coefficient (R) is used as evaluation indicator with range [-1, 1], widely used to measure

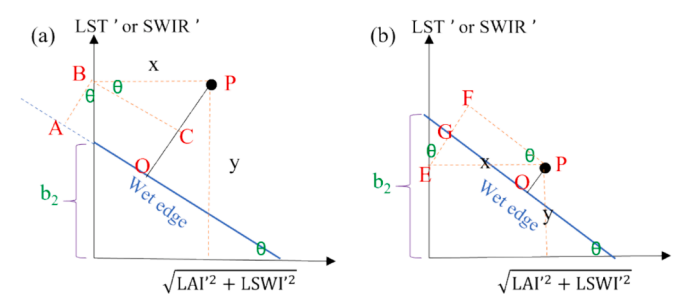


Fig. 7. Illustration of calculating PWSI.

the degree of correlation between two variables, and the larger absolute value indicating the greater correlation (Ly et al., 2018; Cohen et al., 2009). The choice of Pearson Correlation Coefficient for this analysis is justified for several reasons. First, it is a well-established measure for linear relationships, which is appropriate for our study since we expect a linear correlation between drought indices and soil moisture content. Pearson Correlation Coefficient is straightforward to interpret and widely recognized in both meteorological and agricultural research for its robustness and simplicity. While other statistical measures such as Spearman's rank correlation coefficient or Kendall's tau could also be considered, these are typically used when the relationship between variables is non-linear or not assumed to be normally distributed. In our dataset, preliminary analysis suggested a predominantly linear relationship between the drought indices and soil moisture content, justifying the use of Pearson Correlation Coefficient. The workflow illustrating the process for developing and validating ECHI, DCHI, PWSI drought indices is shown in Fig. 8.

Among these three indices used for validation, CWSI is built on the principle of surface energy balance, fully considering the underlying vegetation cover and meteorological factors such as ground wind speed, water vapor pressure, sunshine time, and temperature (Jackson et al., 1988; Idso et al., 1981). Evapotranspiration is the total water vapor flux transported from the ground to the atmosphere, including vegetation transpiration, evaporation of soil water, trapped precipitation or dew. The sum of surface soil water evaporation and vegetation transpiration is usually designated as actual evapotranspiration (ET) (Gao et al., 2006; Liu et al., 2003; Jackson et al., 1988; Idso et al., 1981), and the estimated evapotranspiration under sufficient water supply condition is defined as

potential evapotranspiration (PET) (Liu and Zhang, 2011). The relationship between ET and PET can be an important indicator of crop water scarcity and drought in the region (Ciężkowski et al., 2020; Mu et al., 2011). When the soil is not lacking in water, the actual evapotranspiration is equal to the potential evapotranspiration under ideal conditions, so the CWSI value is 0. When the soil is seriously short of water, the actual evapotranspiration is much smaller than the potential evapotranspiration, and the CWSI value is close to 1. That is to say, the greater the CWSI value is, the more arid the soil is.

TVDI is widely used for monitoring regional soil moisture status and proving drought index construction (Javed et al., 2021). In terms of the theory of vegetation soil line, it introduces surface temperature and structures a triangular feature space in the light of different spectral information of bare soil areas and vegetation covered areas in remote sensing images (Ali et al., 2019; Sandholt et al., 2002). TVDI value ranges from 0 to 1, with smaller values being wetter.

VHI is calculated by Vegetation Condition Index (VCI) and Temperature Condition Index (TCI) (Kogan, 2001; Anderson et al., 2013), which can simultaneously reveal changes in water and temperature in the region. When crops are affected by agricultural drought, VCI and TCI have their own advantages in reflecting crop growth and Thermal Regime (Gidey et al., 2018; Bayarjargal et al., 2006). As drought occurs, vegetation growth is threatened, and the VCI decreases (Sun et al., 2023). In addition, the emergence of agricultural drought is ordinarily accompanied by an abnormal increase in temperature, and the TCI declines (Berry et al., 2010). Consequently, the smaller the VHI, the drier and less healthy the crop.

4. Results and analysis

4.1. Parameterization of ECHI, DCHI, PWSI

Among our proposed three triangular spectral indices, ECHI is calculated directly using formula (2). However, DCHI and PWSI are calculated differently, which are calculated within the feature space of LST' or SWIR' with $\sqrt{LAI'^2+LSWI'^2}$ and required to fit the dry and wet edges. As suggested by Sadeghi et al. (2017), the elimination of oversaturated or shadowed pixels around the edges is achieved through "visual inspection" of pixel distribution. This process helps to precisely define and calculate the equations for dry and wet edges. To create DCHI

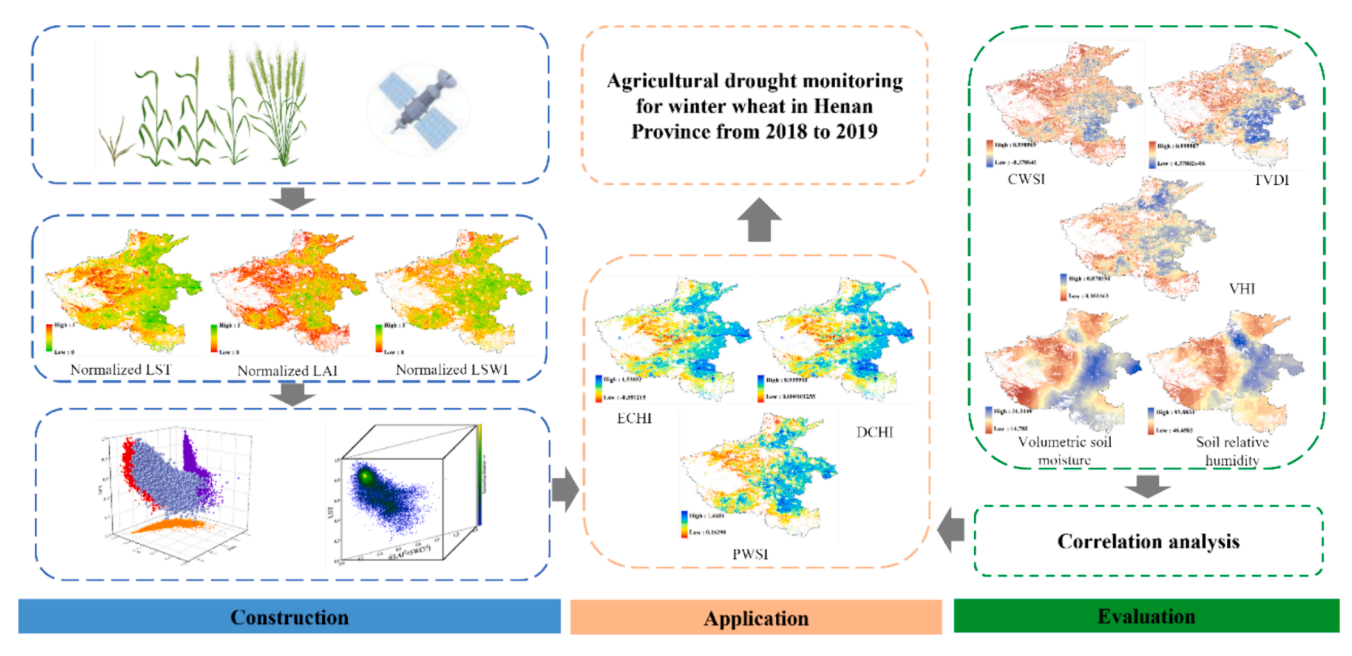


Fig. 8. Flowchart illustrating the process for developing and validating ECHI, DCHI, PWSI drought indices.

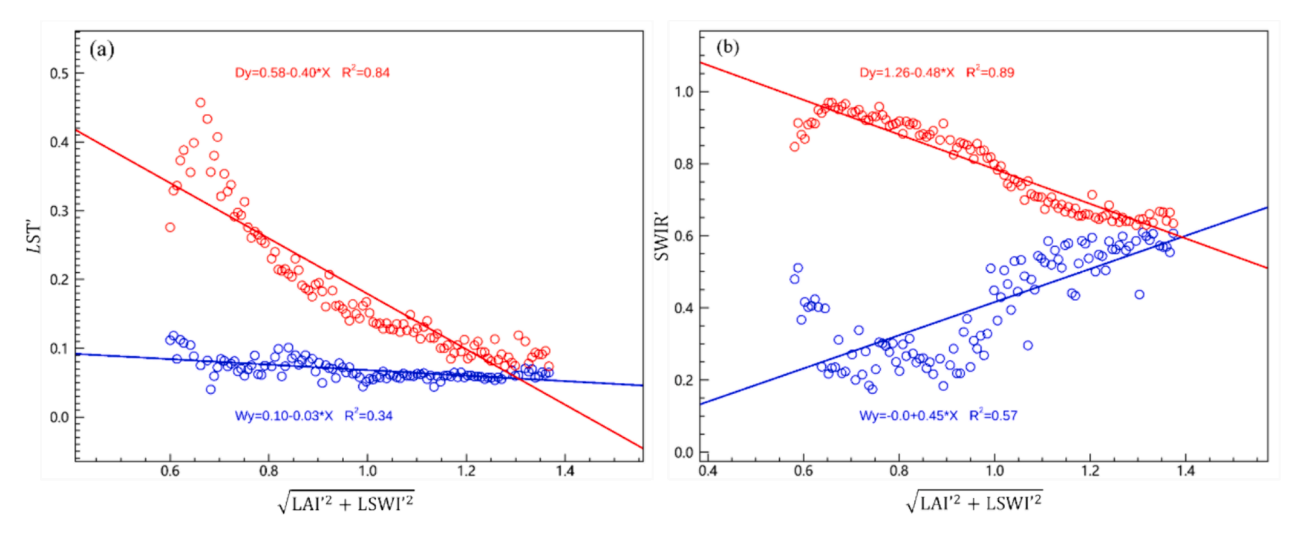


Fig. 9. Diagram of fitted dry and wet edges. (a) fitted dry and wet edges of LST'; (b) fitted dry and wet edges of SWIR'. Notes: The red and blue points are the highest and lowest observed LST' or SWIR' in the boxes of $\sqrt{\text{LA}V^2 + \text{LSW}V^2}$. The red line (dry edge) is the best-fitted line to these highest LST' or SWIR' points, and the blue line (wet edge) is the best-fitted line to those lowest LST' or SWIR' points. (For interpretation of the references to color in this figure legend, the reader is referred to the web version of this article.)

and PWSI, the value of LAI' or SWIR' are categorized into distinct bins on the Y-axis, and the number of bins was determined using formula (3). Subsequently, within each bin of $\sqrt{\text{LAI'}^2 + \text{LSWI'}^2}$, the highest and lowest LST' or SWIR' values will be identified. These points are then subjected to linear regression to establish corresponding regression lines. The fitted dry edge and wet edge for monitoring the typical drought in Henan Province on March 14th, 2019, are shown in Fig. 9.

4.2. Validation using measured soil water content in agricultural meteorological stations

The performance of our proposed ECHI, PWSI, DCHI are validated using the measured RSM and VWC in agricultural meteorological stations. Firstly, we compare the individual SWIR, LAI, LST, LSWI with measured RSM (Fig. 10 (a–d)) and VWC (Fig. 10 (e–h)) in agricultural meteorological stations. Fig. 10 and Table 1 reveal that the individual parameter including SWIR, LAI, LST, LSWI are correlated with measured RSM and VWC with lower correlation coefficient (R) ranging from 0.33

Table 1The absolute value of correlation coefficients between individual SWIR, LAI, LST, LSWI, proposed indices including ECHI, PWSI, DCHI, existing CWSI, TVDI, VHI with measured RSM and VWC.

	SWIR	LAI	LSWI	LST	ECHI ₁	PWSI ₁	DCHI ₁
RSM	0.33	0.41	0.47	0.30	0.63	0.51	0.48
VWC	0.39	0.42	0.45	0.33	0.64	0.57	0.50
	$ECHI_2$	$PWSI_2$	$DCHI_2$	CWSI	TVDI	VHI	
RSM	0.66	0.54	0.57	0.46	0.35	0.44	
VWC	0.65	0.47	0.51	0.47	0.32	0.39	

to 0.47. Secondly, we compare our proposed two kinds of indices including ECHI, PWSI, DCHI with measured RSM and VWC. Fig. 11 (a–f) is the comparations of calculated ECHI₁, PWSI₁, DCHI₁ in SWIR'-LAI'-LSWI' feature space, and Fig. 11 (g–l) is the comparations of calculated ECHI₂, PWSI₂, DCHI₂ in LST'-LAI'-LSWI' feature space. Fig. 11 and Table 1 reveal that there are higher correlation coefficients ranging from

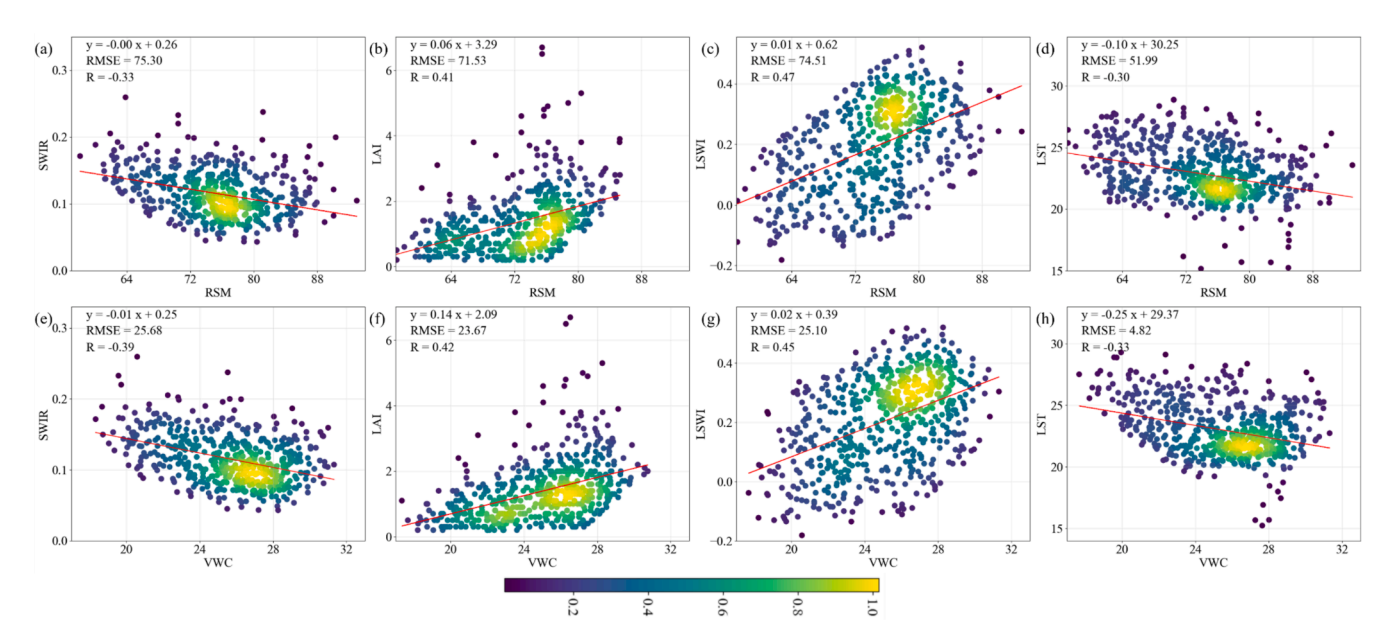


Fig. 10. Comparation of SWIR, LAI, LSWI, LST with measured RSM (a-d) and VWC (e-h). Notes: The color shows the correlation (The same below).

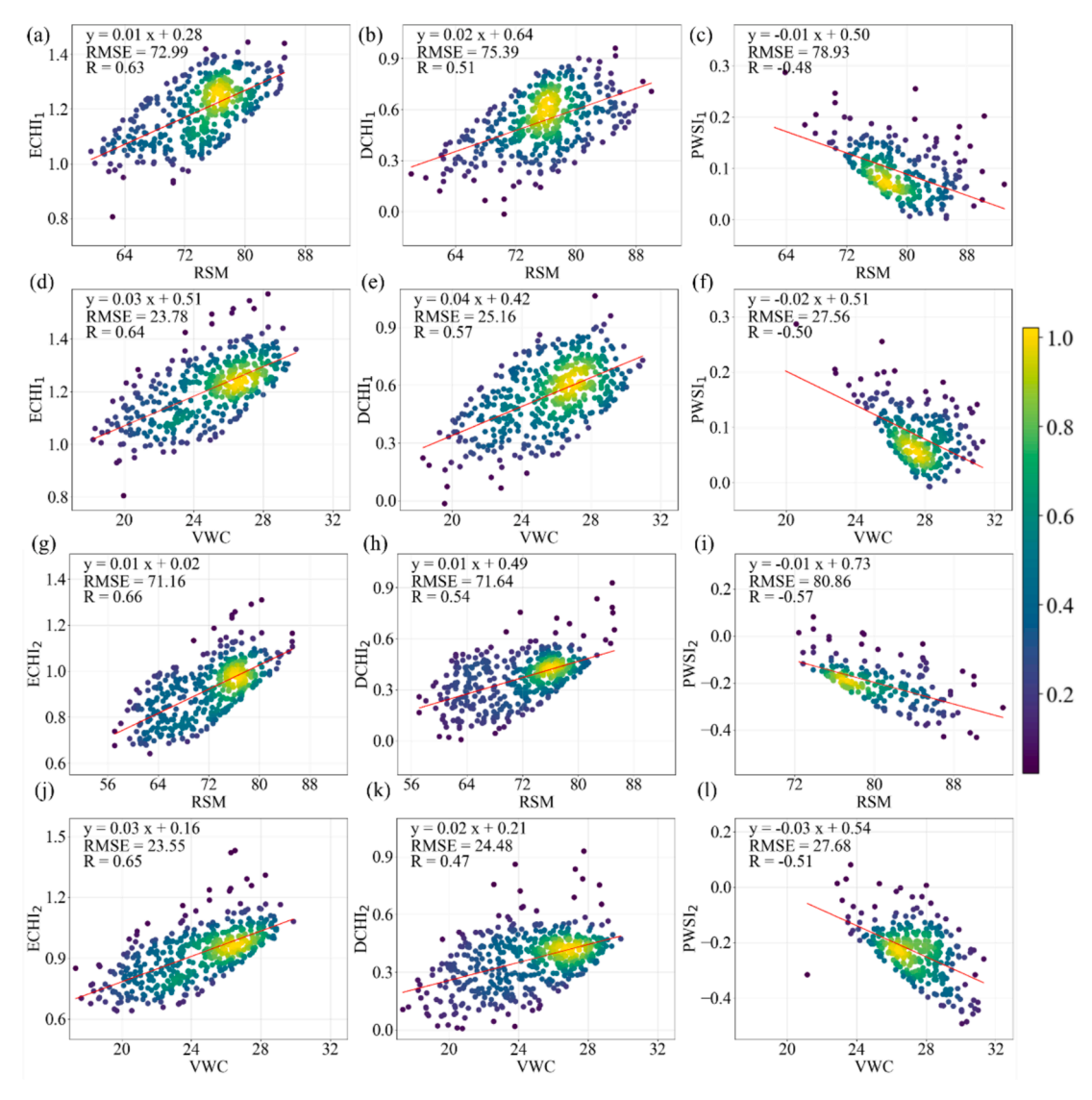


Fig. 11. Comparation of ECHIs, DCHIs, PWSIs resulted from SWIR'-LAI'-LSWI' (a-f) and LST'-LAI'-LSWI' (g-l) with measured RSM and VWC.

0.50 to 0.66 between our proposed ECHI, PWSI, DCHI with measured RSM and VWC. Comparably speaking, there are higher correlation coefficients between calculated ECHI2, PWSI2, DCHI2 using LST'-LAI'-LSWI' feature space than that using ECHI₁, PWSI₁, DCHI₁ feature space. The higher correlation of the ECHI2, PWSI2 and DCHI2 with RSM compared to VWC is an interesting finding that warrants further discussion. Firstly, soil type and structure can affect the relationship between VWC and RSM. For example, soils with a high clay content can hold more water but may not reflect changes in RSM as readily as sandy soils, and soil moisture measurements were taken throughout the study area, with regional variations in soil properties, which affects the correlation with drought indices. Secondly, the methods used to measure RSM and VWC can introduce variability in the data. RSM is derived from soil moisture sensors that measure the dielectric constant of the soil, which is directly influenced by water content. VWC, on the other hand, is derived gravimetric methods or other techniques that can introduce additional uncertainties.

Fig. 12 is the comparation of correlation between existing popular CWSI, TVDI, VHI with measured RSM and VWC. Upon examining Fig. 10, Fig. 11 and Table 1, it becomes evident that our proposed ECHIs, DCHIs, PWSIs are more correlated with measured RSM and VWC in agricultural meteorological stations than the existing popular indices including CWSI, TVDI, VHI. Notably, the validation performance using

RSM is better than that using VWC. Inferring from these findings, it can be concluded that our proposed indices showed higher competitiveness compared with the existing popular drought indices in monitoring soil water content. This conclusion aligns with the outcomes of Liu et al. (2020) shared in Nature Communication, where soil moisture emerged as the predominant factor influencing drought stress in arid and semi-arid regions. Taken together, the results from this study indicate that our proposed indices are effective for drought monitoring.

4.3. Comparison with existing popular drought indices

The spatial consistency and correlation between our proposed ECHIs, DCHIs, PWSIs with popular CWSI, TVDI, VHI are done to explore the performance of our proposed indices in drought monitoring. Fig. 13 is the spatial consistency between them, and Fig. 14 is the correlation between them. Among these three popular drought indices, CWSI is rooted in evapotranspiration principles, primarily capturing the water requirements of crops under drought-induced stress. TVDI and VHI are calculated from NDVI and LST. Due to their significance in drought monitoring, CWSI, TVDI and VHI are served as a benchmark for evaluating the performance of our proposed indices firstly. From the spatial distribution of all these indices, the drought areas monitored by ECHI is consistent with that showed by CWSI, especially for ECHI₂. CWSI and

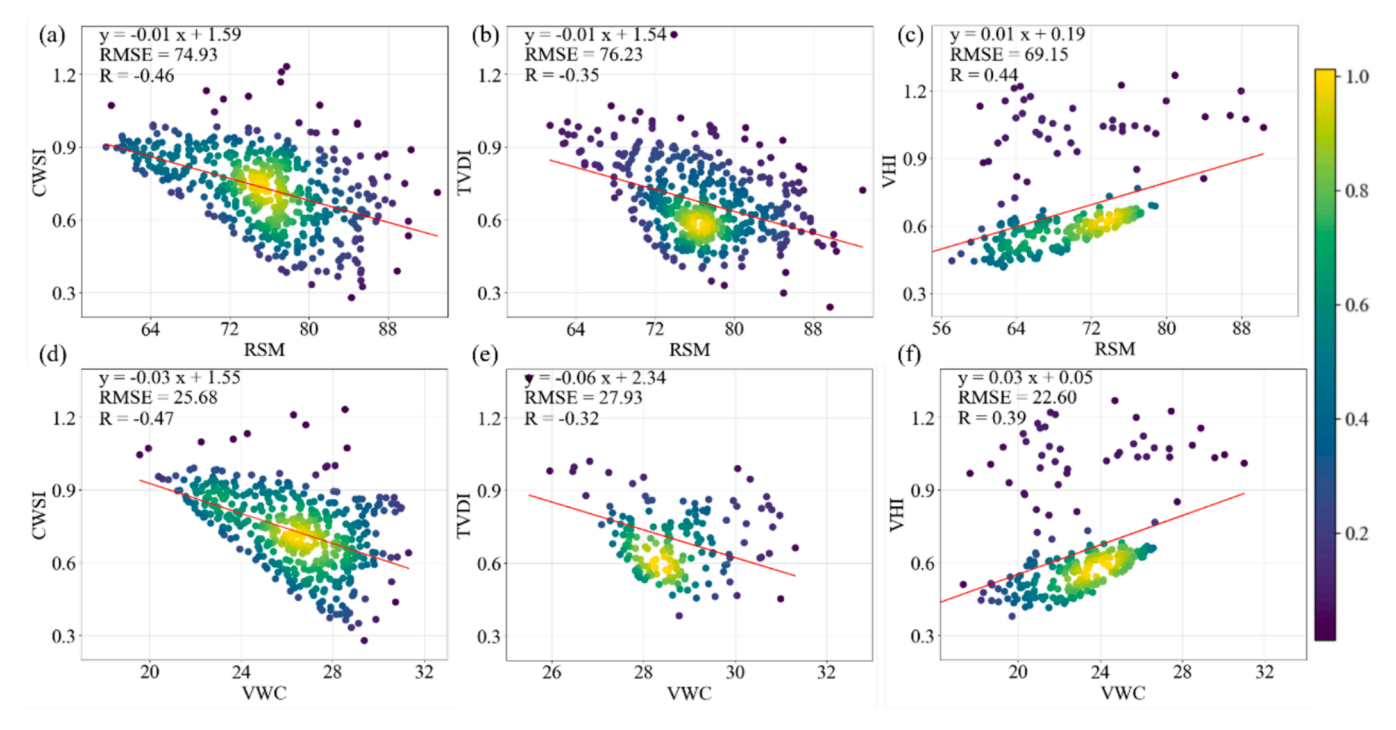


Fig. 12. Comparation of existing popular CWSI, TVDI, VHI with measured RSM and VWC.

ECHI $_2$ are divided into quartiles 0th -25th, 25th -50th, 50th -75th, and 75th -100th based on the thresholds, and the proportions of each quartile were, respectively, 1.13 %, 41.24 %, 64.29 %, 1.82 %, 1.04 %, 38.02 %, 59.26 %, 1.67 %. Comparably speaking, DCHIs and PWSIs are more consistent with TVDI and VHI, respectively. And PWSI $_1$ is more consistent with VHI. From the spatial perspective, the spatial characteristics of ECHIs, DCHIs, PWSIs exhibited strong similarities with CWSI, TVDI, VHI. These three triangular spectral indices effectively reflected the soil moisture content response to drought conditions. Comparably speaking, ECHI $_2$, DCHI $_2$, CWSI, TVDI monitor more drought areas than that of ECHI $_1$, DCHI $_1$, PWSI $_1$, PWSI $_2$, VHI.

Through spatial comparisons of ECHIs, DCHIs, PWSIs, with CWSI, TVDI, VHI, it can be observed that the areas characterized as droughtprone by ECHIs, DCHIs, and PWSIs generally align with those indicated by three popular drought monitoring indices including CWSI, TVDI and VHI. The quantitative validation is carried out by correlation analysis for assessing the meteorological drought monitoring capability of our proposed spectral indices. Among all these absolute values of correlation coefficients between our proposed indices and popular CWSI, TVDI, VHI, our proposed ECHI2, DCHI2, PWSI2 calculated in LST'-LAI'-LSWI' feature space are with the highest correlation coefficients with VHI of 0.93, 0.74 and 0.95 respectively. Comparably speaking, the correlation coefficient between our ECHI1, DCHI1, PWSI1 with TVDI are lowest with 0.71, 0.59 and 0.68, respectively. Generally speaking, our proposed ECHIs, DCHIs, PWSIs spectral indices are with the highest correlation with VHI, and after it is CWSI, and the index with the lowest correlation is TVDI.

4.4. Drought monitoring in a whole drought process of winter wheat

Taking into account the enhanced drought monitoring capabilities and effectiveness of the $\rm ECHI_2$ within the proposed three-dimensional drought indices, an agricultural drought assessment was conducted in the study area spanning from 2018 to 2019 (using 16-day combined $\rm ECHI_2$). The primary objective was to recreate the progression of drought throughout the complete growth period of winter wheat. Fig. 15 (a–b) illustrates the spatial and temporal variations of $\rm ECHI_2$ throughout the entire growth period of winter wheat, revealing that drought

conditions are pervasive across Henan Province, with a significant concentration in the southwest, central, and eastern regions. Notably, October 2018 exhibited the broadest and most intense drought conditions in the province, coinciding with the winter wheat sowing period. During this time, reduced vegetation cover and canopy water content were observed, with ECHI2 values primarily reflecting surface temperature conditions. By the end of December 2018, drought conditions in wheat planting areas had gradually alleviated, with no drought reported in other regions, except for mild drought in areas with inadequate soil moisture. A downward trend in ECHI2 occurred between January 2019 and early February 2019 (there were missing data during this period, so this may have increased the error in the drought assessment), which suggests that mild drought was occurring in some regions, mainly concentrated in the southwest and southern regions. Subsequently, ECHI2 exhibited an upward trend, with no drought in most parts of the province, except for poor soil moisture in the western and southwestern regions. In April 2019, ECHI2 reached its peak for the year, correlating with widespread rainfall during that month, indicating that the ECHI2 index accurately depicts the impact of precipitation. From late April to early June 2019, ECHI2 decreased, indicating drought in most regions of the province, particularly in early June. During this late growth stage of winter wheat, a decrease in LAI, plant water content, and an increase in temperature were observed, with ECHI2 values primarily reflecting surface temperature conditions. The lack of precipitation during this period also led to mild drought in the central, western, southwestern, and northern parts of the province. These findings align with the monthly water condition reports from the Henan Provincial Hydrology and Water Resources Measurement Center (https://www.hnssw.com. cn), enhancing the credibility of ECHI2-based drought monitoring and confirming its efficacy in capturing the onset, development, and cessation of drought events.

5. Discussions

5.1. Potential improvements for agricultural drought monitoring

Although it is revealed that ECHIs, PWSIs, and DCHIs outperform three popular drought indices including CWSI, TVDI and VHI in

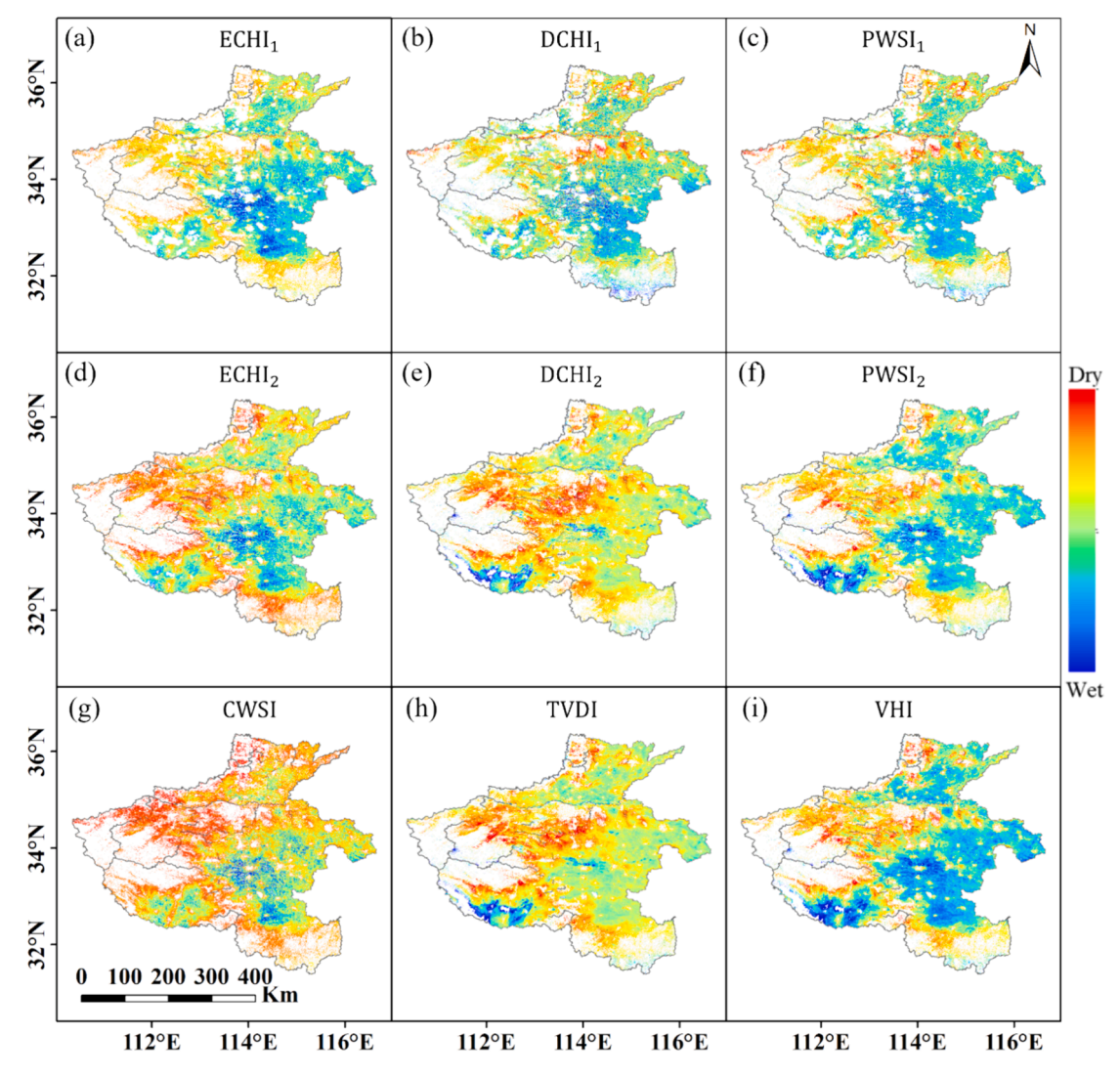


Fig. 13. Spatial consistency of ECHIs, DCHIs, PWSIs (a-f) with CWSI (g), TVDI (h), VHI (i) used for drought monitoring of winter wheat in Henan Province on March 14th, 2019. Notes: ECHI₁, DCHI₂, PWSI₂ are calculated in LST'-LAI'-LSWI' feature space, and ECHI₂, DCHI₂, PWSI₂ are calculated in LST'-LAI'-LSWI' feature space (The same below).

agricultural drought monitoring in this study, their correlation with meteorological station data is exceptionally low. There are still some issues for further exploration. Firstly, it's important to note that the relationship between LST, LAI, LSWI, and soil moisture is not strictly linear. As illustrated in Fig. 3, the distributions of soil water in LST-LAI, LAI-LSWI and LST-LSWI spaces tend to form trapezoids or triangles, rather than following a straightforward linear pattern. The further studies could fit more nonlinear models to capture these non-linear responses of agricultural drought. Specific non-linear models that might be explored include polynomial regression, support vector machines with non-linear kernels, and artificial neural networks. These models can better capture the complexities in the relationships between the drought indices and soil moisture. Moreover, the accuracy of drought monitoring is contingent on the retrieving accuracy of LST, LAI and LSWI, as well as the accurate fitting of dry edge and wet edge. Challenges in accurately retrieving these parameters can introduce errors that affect the performance of drought indices. Additionally, the removal of unnecessary oversaturated or shadowed pixels can aid in defining edges more effectively. Deep learning techniques, such as convolutional neural networks (CNN) and generative adversarial networks (GAN), could be investigated to achieve this objective. CNN are particularly well-suited for image data and could be used to improve the accuracy of LST, LAI, and LSWI retrievals. By training on large datasets

of satellite images and corresponding ground-truth measurements, CNN could learn to correct for atmospheric distortions, sensor noise, and other factors that affect the retrieval accuracy. GAN can be used to generate high-quality synthetic data that can supplement real data in training models, especially in cases where ground-truth data is sparse. This can help in refining the edges and improving the accuracy of the drought indices. GAN can also be employed to enhance the resolution of satellite images, making it easier to identify and remove oversaturated or shadowed pixels. These techniques are capable of handling complex data processing tasks and could improve the accuracy and reliability of the drought indices. One issue to point out is that there are two feature spaces are built in this study including LST'-LAI'-LSWI' and SWIR'-LAI'-LSWI'. The validation results in Section 4.2 and Section 4.3 reveal that the monitored results of winter wheat using LST'-LAI'-LSWI' are closer to measured RSM and VWC in agricultural meteorological stations than that using SWIR'-LAI'-LSWI'. However, we still encourage the usage of SWIR'-LAI'-LSWI' for agricultural drought monitoring because the acquisition of SWIR reflectance is easy and quick without the error propagation and difficulties of LST retrieval.

5.2. Field management

As we all know that there is difference for the drought response of

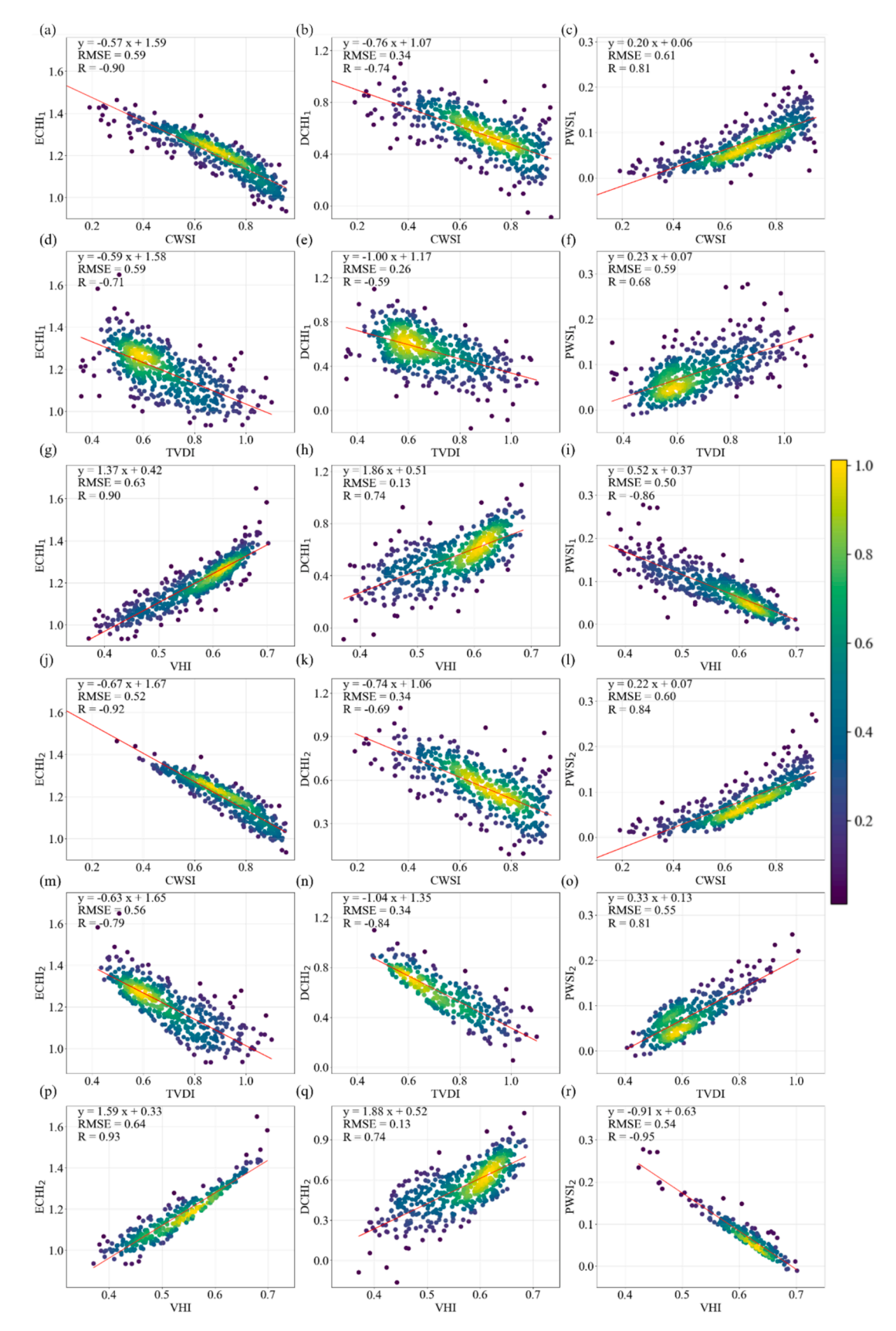


Fig. 14. ECHIs, DCHIs, PWSIs in SWIR'-LAI'-LSWI' feature space (a-i) and in LST'-LAI'-LSWI' feature space (j-r) with popular CWSI, TVDI, VHI.

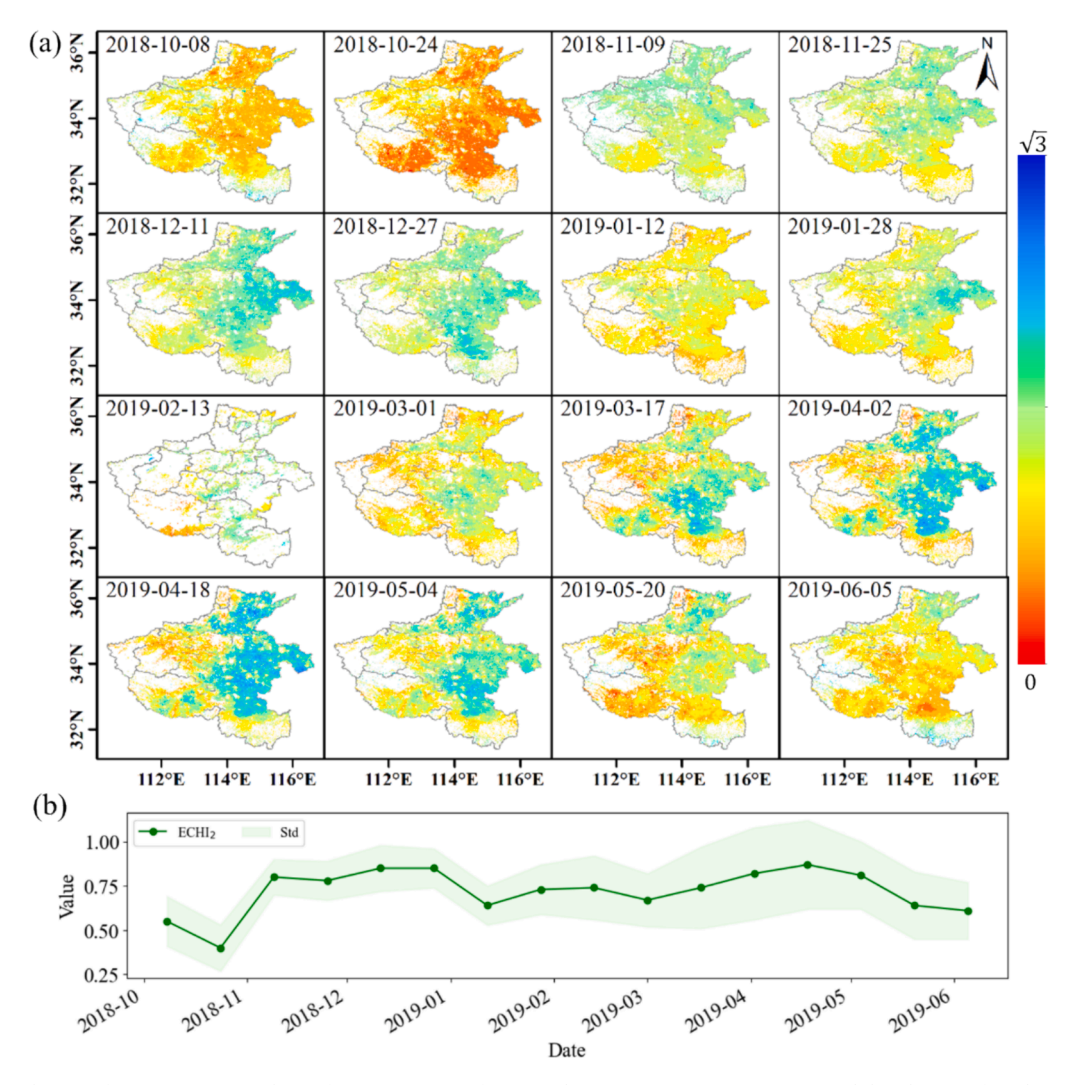


Fig. 15. Spatial distribution of ECHI₂ in winter wheat of Henan Province from October 2018 to June 2019. (a) Spatial distribution of 16-day combined ECHI₂; (b) Time-series variation curves of ECHI₂ and fitted trend line.

winter wheat in rainfed and irrigation areas. Therefore, we compare the performance of our proposed spectral indices both in rainfed cropland and irrigation cropland. Considering there is the best performance of ECHI2 index calculated in LST'-LAI'-LSWI' feature space for drought monitoring, we compare and analyse ECHI2 for the comparation in rainfed cropland and irrigation cropland. Fig. 16 is the comparation of ECHI2 in rainfed cropland and irrigation cropland with measured RSM and VWC in agricultural meteorological stations. The correlation between ECHI2 with RSM and VWC in irrigation area are lower in rainfed area, with the correlation coefficient of 0.59 and 0.56, 0.68 and 0.65 respectively shown in Fig. 16. Fig. 17 reveals that there is more severe drought in rainfed cropland than that in irrigation cropland. And the irrigation management plays an important role in alleviating crop drought. The difference in ECHI2 performance between rainfed and irrigated cropland can be attributed to several factors. In irrigated areas, the controlled water supply can mitigate the effects of drought, leading to less variation in soil moisture and vegetation water content. This results in a less pronounced signal for the ECHI2 to detect drought conditions. Conversely, rainfed areas are more directly affected by natural precipitation patterns, which cause more significant variations in soil moisture and crop water stress, leading to higher sensitivity of the ECHI₂. The physiological response of winter wheat to drought stress can differ between rainfed and irrigated systems. In rainfed systems, crops are more likely to exhibit stress symptoms such as reduced leaf area and lowered canopy water content, which are detectable by spectral indices.

In contrast, irrigation can buffer these stress symptoms, making it harder for spectral indices to distinguish between water-stressed and non-stressed states. Irrigation can create microclimatic conditions that differ from those in rainfed areas, such as increased humidity and lower soil surface temperatures. These conditions can affect the thermal and spectral properties of the crop canopy, influencing the performance of indices that rely on LST.

6. Conclusions

Agricultural drought threatens food security and agricultural sustainable development. We propose three novel triangular spectral indices including ECHIs, DCHIs and PWSIs for characterizing winter wheat drought in this study. The comparation of ECHIs, DCHIs, PWSIs with measured RSM and VWC in agricultural meteorological stations and existing popular drought indices including CWSI, TVDI and VHI are done. Our findings are as follows.

(1) The integration of LAI, LSWI and LST or SWIR as the proxies of crop growth, crop canopy water content and canopy temperature does good to improve crop drought monitoring. All the comparations of proposed ECHIs, DCHIs, PWSIs with measured RSM, VWC and existing CWSI, TVDI, VHI prove the improvement of ECHI, DCHI, PWSI for drought characterizing.

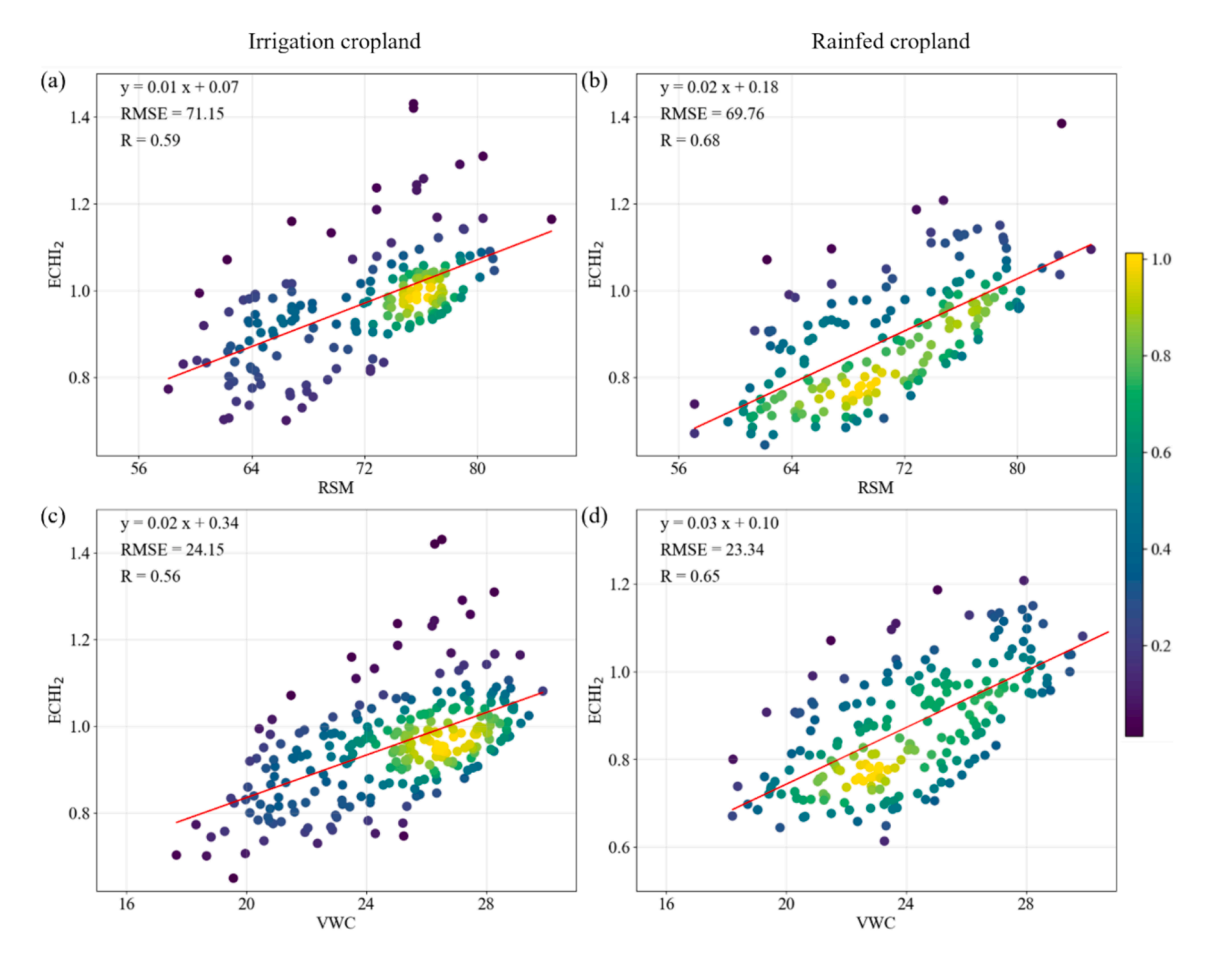


Fig. 16. Comparation of ECHI₂ in rainfed cropland and irrigation cropland with measured RSM and VWC in agricultural meteorological stations. (a) Comparation of ECHI₂ in irrigation cropland with measured RSM; (b) Comparation of ECHI₂ in rainfed cropland with measured RSM; (c) Comparation of ECHI₂ in irrigation cropland with measured VWC; (d) Comparation of ECHI₂ in rainfed cropland with measured VWC.

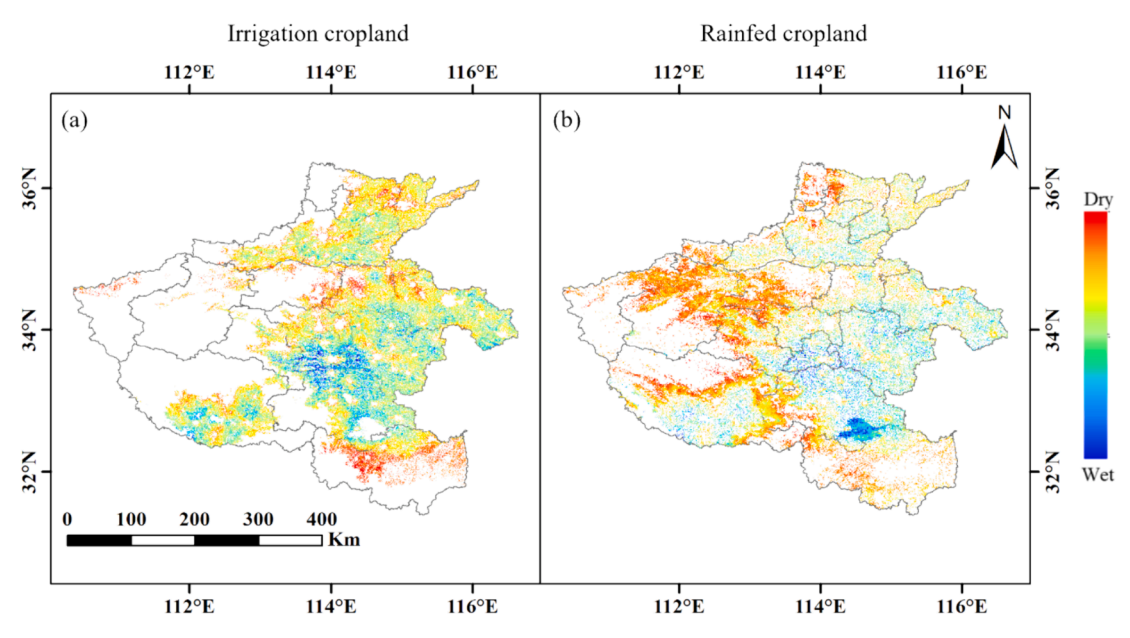


Fig. 17. Spatial distribution of ECHI₂ for drought monitoring in irrigation and rainfed cropland. (a) ECHI₂ for drought monitoring in irrigation cropland; (b) ECHI₂ for drought monitoring in rainfed cropland.

- (2) Our proposed drought indices including ECHIs, DCHIs, PWSIs demonstrate robust capabilities in a complete drought process in Henan Province in 2019. Furtherly, the performance of these triangular spectral indices is validated both in irrigation cropland and rainfed cropland.
- (3) The proposed indices show enhanced sensitivity to changes in soil moisture and crop water status, particularly in the integration of multiple spectral features. This leads to more accurate detection and monitoring of drought conditions. Meanwhile, by considering the non-linear relationships between LST, LAI, and LSWI, the indices better capture the complex interactions occurring during drought conditions, compared to the linear models used in indices like CWSI, TVDI, and VHI. And the indices perform well across different types of cropland (irrigated and rainfed), indicating their broad applicability.
- (4) The accuracy of the proposed indices is contingent on the precise retrieval of LST, LAI, and LSWI. Errors in these retrievals can propagate and affect the drought monitoring accuracy. This is particularly challenging due to atmospheric distortions and sensor calibration issues. The need for high-quality, frequent satellite observations to retrieve the necessary spectral data can be a limitation in regions with persistent cloud cover or limited satellite coverage.

CRediT authorship contribution statement

Fu Xuan: Writing – original draft, Methodology, Conceptualization, Data curation, Software, Visualization. Hui Liu: Writing – original draft, Methodology, Visualization. JingHao Xue: Investigation, Resources. Ying Li: Validation, Resources. Junming Liu: Resources, Writing – review & editing. Xianda Huang: Software, Data curation. Zihao Tan: Investigation, Resources. Mohamed A.M. Abd Elbasit: Conceptualization, Investigation. Xiaohe Gu: Investigation, Validation. Wei Su: Writing – review & editing, Methodology, Funding acquisition, Conceptualization.

Declaration of competing interest

The authors declare that they have no known competing financial interests or personal relationships that could have appeared to influence the work reported in this paper.

Data availability

Data will be made available on request.

Acknowledgment

This work was supported by the National Key R&D Program Project (No. 2022YFD2001103), the National Natural Science Foundation of China under the project (No. 42171331), the 2115 Talent Development Program of China Agricultural University and the National Natural Science Foundation of China (41805090).

References

- Abbass, K., Qasim, M.Z., Song, H., Murshed, M., Mahmood, H., Younis, I., 2022. A review of the global climate change impacts, adaptation, and sustainable mitigation measures. Environ. Sci. Pollut. Res. 29 (28), 42539–42559.
- Ali, S., Tong, D., Xu, Z.T., Henchiri, M., Wilson, K., Siqi, S., Zhang, J., 2019. Characterization of drought monitoring events through MODIS-and TRMM-based DSI and TVDI over South Asia during 2001–2017. Environ. Sci. Pollut. Res. 26, 33568–33581.
- Anderson, M.C., Hain, C., Otkin, J., Zhan, X., Mo, K., Svoboda, M., Wardlow, B., Pimstein, A., 2013. An intercomparison of drought indicators based on thermal remote sensing and NLDAS-2 simulations with US Drought Monitor classifications. J. Hydrometeorol. 14 (4), 1035–1056.
- Anees, S.A., Mehmood, K., Khan, W.R., Sajjad, M., Alahmadi, T.A., Alharbi, S.A., Luo, M., 2024. Integration of machine learning and remote sensing for above ground biomass

- estimation through Landsat-9 and field data in temperate forests of the Himalayan region. Eco. Inform. 82, 102732 https://doi.org/10.1016/j.ecoinf.2024.102732.
- Azmi, M., Rüdiger, C., Walker, J.P., 2016. A data fusion-based drought index. Water Resour. Res. 52 (3), 2222–2239.
- Bayarjargal, Y., Karnieli, A., Bayasgalan, M., Khudulmur, S., Gandush, C., Tucker, C.J., 2006. A comparative study of NOAA–AVHRR derived drought indices using change vector analysis. Remote Sens. Environ. 105 (1), 9–22.
- Berry, J.A., Beerling, D.J., Franks, P.J., 2010. Stomata: key players in the earth system, past and present. Curr. Opin. Plant Biol. 13 (3), 232–239.
- Carlson, T.N., Gillies, R.R., Perry, E.M., 1994. A method to make use of thermal infrared temperature and NDVI measurements to infer surface soil water content and fractional vegetation cover. Remote Sens. Rev. 9, 161–173. https://doi.org/ 10.1080/02757259409532220.
- Ciężkowski, W., Szporak-Wasilewska, S., Kleniewska, M., Jóźwiak, J., Gnatowski, T., Dąbrowski, P., Góraj, M., Szatyłowicz, J., Ignar, S., Chormański, J., 2020. Remotely sensed land surface temperature-based water stress index for wetland habitats. Remote Sens. 12 (4), 631.
- Cohen, I., Huang, Y., Chen, J., Benesty, J., Benesty, J., Chen, J., Huang, Y., Cohen, I., 2009. Pearson correlation coefficient. Noise Reduction in Speech Processing 1–4.
- Dai, A., 2011. Drought under global warming: a review. Wiley Interdiscip. Rev. Clim. Chang. 2 (1), 45–65.
- Dong, H., Pengxin, W., Yue, Z., Huiren, T., Xijia, Z., 2021. Progress of agricultural drought monitoring and forecasting using satellite remote sensing. Smart Agriculture 3 (2), 1.
- Dubovyk, O., Ghazaryan, G., González, J., Graw, V., Löw, F., Schreier, J., 2019. Drought hazard in Kazakhstan in 2000–2016: a remote sensing perspective. Environ. Monit. Assess. 191, 1–17.
- Esch, S., Korres, W., Reichenau, T.G., Schneider, K., 2018. Soil moisture index from ERS-SAR and its application to the analysis of spatial patterns in agricultural areas.

 J. Appl. Remote Sens. 12 (2), 022206.
- Fang, W., Huang, S., Huang, Q., Huang, G., Wang, H., Leng, G., Wang, L., Guo, Y., 2019. Probabilistic assessment of remote sensing-based terrestrial vegetation vulnerability to drought stress of the Loess Plateau in China. Remote Sens. Environ. 232, 111290 https://doi.org/10.1016/j.rse.2019.111290.
- FAO. 2023. The Impact of Disasters on Agriculture and Food Security 2023 Avoiding and reducing losses through investment in resilience. Rome. 10.4060/cc7900en.
- Fensholt, R., Sandholt, I., 2003. Derivation of a shortwave infrared water stress index from MODIS near-and shortwave infrared data in a semiarid environment. Remote Sens. Environ. 87 (1), 111–121.
- Gao, G., Chen, D.L., Ren, G.Y., Chen, Y., Liao, Y.M., 2006. Trend of potential evapotranspiration over China during 1956 to 2000. Geogr. Res. 25 (3), 378–387.
- Gidey, E., Dikinya, O., Sebego, R., Segosebe, E., Zenebe, A., 2018. Analysis of the longterm agricultural drought onset, cessation, duration, frequency, severity and spatial extent using vegetation health index (VHI) in Raya and its environs, Northern Ethiopia. Environmental Systems Research 7, 1–18.
- Gutman, G.G., 1990. Towards monitoring droughts from space. J. Clim. 3 (2), 282–295.
 Ha, T.V., Uereyen, S., Kuenzer, C., 2023. Agricultural drought conditions over mainland Southeast Asia: spatiotemporal characteristics revealed from MODIS-based vegetation time-series. Int. J. Appl. Earth Obs. Geoinf. 121, 103378.
- vegetation time-series. Int. J. Appl. Earth Obs. Geoinf. 121, 103378.
 Hao, Z., Singh, V.P., 2015. Drought characterization from a multivariate perspective: a review. J. Hydrol. 527, 668–678.
- Henan Provincial Bureau Of Statistics, 2019.
- Huang, X., Huang, J., Li, X., Shen, Q., Chen, Z., 2022. Early mapping of winter wheat in Henan province of China using time series of Sentinel-2 data. Gisci. Remote Sens. 59 (1), 1534–1549.
- Huang, J., Ma, H., Sedano, F., Lewis, P., Liang, S., Wu, Q., Su, W., Zhang, X., Zhu, D., 2019. Evaluation of regional estimates of winter wheat yield by assimilating three remotely sensed reflectance datasets into the coupled WOFOST-PROSAIL model. Eur. J. Agron. 102, 1–13. https://doi.org/10.1016/j.eja.2018.10.008.
- Idso, S.B., Jackson, R.D., Pinter Jr, P.J., Reginato, R.J., Hatfield, J.L., 1981. Normalizing the stress-degree-day parameter for environmental variability. Agric. Meteorol. 24, 45–55.
- Jackson, R.D., Kustas, W.P., Choudhury, B.J., 1988. A reexamination of the crop water stress index. Irrig. Sci. 9, 309–317.
- Javed, T., Li, Y., Rashid, S., Li, F., Hu, Q., Feng, H., Chen, X., Ahmad, S., Liu, F., Pulatov, B., 2021. Performance and relationship of four different agricultural drought indices for drought monitoring in China's mainland using remote sensing data. Sci. Total Environ. 759, 143530.
- Joshi, R.C., Ryu, D., Sheridan, G.J., Lane, P.N., 2021. Modeling vegetation water stress over the forest from space: Temperature Vegetation Water Stress Index (TVWSI). Remote Sens. 13 (22), 4635.
- Kogan, F.N., 1995. Application of vegetation index and brightness temperature for drought detection. Adv. Space Res. 15 (11), 91–100.
- Kogan, F.N., 2001. Operational space technology for global vegetation assessment. Bull. Amer. Meteorol. Soc. 82 (9), 1949–1964.
- Lesk, C., Anderson, W., Rigden, A., Coast, O., Jägermeyr, J., McDermid, S., Davis, K.F., Konar, M., 2022. Compound heat and moisture extreme impacts on global crop yields under climate change. Nat. Rev. Earth Environ. 3 (12), 872–889.
- Li, X., Wu, J., Lv, A., Liu, M., 2013. The difference of drought impacts on winter wheat leaf area index under different CO2 concentration. Acta Ecol. Sin. 33 (9), 2023.
- Li, Z., Xuan, F., Dong, Y., Huang, X., Liu, H., Zeng, Y., Su, W., Huang, J., Li, X., 2024. Performance of GEDI data combined with Sentinel-2 images for automatic labelling of wall-to-wall corn mapping. Int. J. Appl. Earth Obs. Geoinf. 127, 103643 https:// doi.org/10.1016/j.jag.2023.103643.

- Liu, J., Chen, J.M., Cihlar, J., 2003. Mapping evapotranspiration based on remote sensing: an application to Canada's landmass. Water Resour. Res. 39 (7).
- Liu, L., Gudmundsson, L., Hauser, M., Qin, D., Li, S., Seneviratne, S.I., 2020. Soil moisture dominates dryness stress on ecosystem production globally. Nat. Commun. 11 (1), 4892.
- Liu, C., Zhang, D., 2011. Temporal and spatial change analysis of the sensitivity of potential evapotranspiration to meteorological influencing factors in China. Acta Geograph. Sin. 66 (5), 579–588.
- Luo, M., Anees, S.A., Huang, Q., Qin, X., Qin, Z., Fan, J., Han, G., Zhang, L., Shafri, H.Z. M., 2024. Improving forest above-ground biomass estimation by integrating individual machine learning models. Forests 15, 975. https://doi.org/10.3390/f15060975
- Ly, A., Marsman, M., Wagenmakers, E.J., 2018. Analytic posteriors for Pearson's correlation coefficient. Stat. Neerl. 72 (1), 4–13.
- Ma Rufah, U., Hidayat, R., Prasasti, I., 2017. Analysis of relationship between meteorological and agricultural drought using standardized precipitation index and vegetation health index. In: IOP Conference Series: Earth and Environmental Science. IOP Publishing, p. 012008.
- Mehmood, K., Anees, S.A., Luo, M., Akram, M., Zubair, M., Khan, K.A., Khan, W.R., 2024a. Assessing Chilgoza Pine (*Pinus gerardiana*) forest fire severity: remote sensing analysis, correlations, and predictive modeling for enhanced management strategies. Trees, Forests and People 16, 100521. https://doi.org/10.1016/j.tfp.2024.100521.
- Mehmood, K., Anees, S.A., Rehman, A., Pan, S., Tariq, A., Zubair, M., Liu, Q., Rabbi, F., Khan, K.A., Luo, M., 2024b. Exploring spatiotemporal dynamics of NDVI and climate-driven responses in ecosystems: Insights for sustainable management and climate resilience. Eco. Inform. 80, 102532 https://doi.org/10.1016/j.ecoinf.2024.102532.
- Moran, M.S., Clarke, T.R., Inoue, Y., Vidal, A., 1994. Estimating crop water deficit using the relation between surface-air temperature and spectral vegetation index. Remote Sens. Environ. 49, 246–263. https://doi.org/10.1016/0034-4257(94)90020-5.
- Mu, Q., Zhao, M., Running, S.W., 2011. Improvements to a MODIS global terrestrial evapotranspiration algorithm. Remote Sens. Environ. 115 (8), 1781–1800.
- Sadeghi, M., Babaeian, E., Tuller, M., Jones, S.B., 2017. The optical trapezoid model: a novel approach to remote sensing of soil moisture applied to Sentinel-2 and Landsat-8 observations. Remote Sens. Environ. 198, 52–68.
- Sandholt, I., Rasmussen, K., Andersen, J., 2002. A simple interpretation of the surface temperature/vegetation index space for assessment of surface moisture status. Remote Sens. Environ. 79 (2–3), 213–224.
- Sheffield, J., Wood, E.F., 2012. Drought: past problems and future scenarios. Routledge. Shi, X., Ding, H., Wu, M., Zhang, N., Shi, M., Chen, F., Li, Y., 2022. Effects of different types of drought on vegetation in Huang-Huai-Hai River Basin. China. Ecol. Indic. 144, 109428.
- Sturges, H.A., 1926. The choice of a class interval. J. Am. Stat. Assoc. 21 (153), 65-66.

- Sun, N., Chen, Q., Liu, F., Zhou, Q., Guo, Y., 2023. Agricultural drought research in Yellow River-Huangshui River Valley from 2000 to 2020. Arid Area Geography 46 (3), 437–447.
- Wang, L., Qu, J.J., Hao, X., Zhu, Q., 2008. Sensitivity studies of the moisture effects on MODIS SWIR reflectance and vegetation water indices. Int. J. Remote Sens. 29 (24), 7065–7075.
- Wei, W., Pang, S., Wang, X., Zhou, L., Xie, B., Zhou, J., Li, C., 2020. Temperature vegetation precipitation dryness index (TVPDI)-based dryness-wetness monitoring in China. Remote Sens. Environ. 248, 111957.
- Wilhite, D.A., Glantz, M.H., 1985. Understanding: the drought phenomenon: the role of definitions. Water Int. 10 (3), 111–120.
- Xu, M., Yao, N., Hu, A., de Goncalves, L.G.G., Mantovani, F.A., Horton, R., Heng, L., Liu, G., 2022. Evaluating a new temperature-vegetation-shortwave infrared reflectance dryness index (TVSDI) in the continental United States. J. Hydrol. 610, 127785
- Xuan, F., Dong, Y., Li, J., Li, X., Su, W., Huang, X., Huang, J., Xie, Z., Li, Z., Liu, H., Tao, W., Wen, Y., Zhang, Y., 2023. Mapping crop type in Northeast China during 2013–2021 using automatic sampling and tile-based image classification. Int. J. of Applied Earth Observation and Geoinformation 117, 103178. https://doi.org/10.1016/j.jag.2022.103178.
- Yihdego, Y., Vaheddoost, B., Al-Weshah, R.A., 2019. Drought indices and indicators revisited. Arab. J. Geosci. 12, 1–12.
- Zhang, C., Dong, J., Ge, Q., 2022a. Mapping 20 years of irrigated croplands in China using MODIS and statistics and existing irrigation products. Sci. Data 9 (1).
- Zhang, C., Dong, J., Ge, Q., 2022b. IrriMap CN: annual irrigation maps across China in 2000–2019 based on satellite observations, environmental variables, and machine learning. Remote Sens. Environ. 280, 113184.
- Zhang, N., Hong, Y., Qin, Q., Liu, L., 2013. VSDI: a visible and shortwave infrared drought index for monitoring soil and vegetation moisture based on optical remote sensing. Int. J. Remote Sens. 34 (13), 4585–4609.
- Zhang, L., Jiao, W., Zhang, H., Huang, C., Tong, Q., 2017. Studying drought phenomena in the Continental United States in 2011 and 2012 using various drought indices. Remote Sens. Environ. 190, 96–106.
- Zhang, Q., Shi, R., Xu, C., Sun, P., Yu, H., Zhao, J., 2022. Multisource data-based integrated drought monitoring index: model development and application. J. Hydrol. 615, 128644.
- Zhang, J., Zhang, Q., Bao, A., Wang, Y., 2019. A new remote sensing dryness index based on the near-infrared and red spectral space. Remote Sens. 11 (4), 456.

Further reading

Henan Province Statistical Bulletin on National Economic and Social Development. 2011.